A 3*D* Statistical Fluid Registration Algorithm

Caroline Brun*[1], Natasha Leporé*[1,5], Xavier Pennec[2], Yi-Yu Chou[1], Agatha D. Lee[1], Greig de Zubicaray[3], Katie McMahon[3], Margaret J. Wright[4], and Paul M. Thompson[1] [* equal contribution]

Abstract. In this paper, we further investigate a Statistically-Assisted Fluid Image Registration Algorithm (SAFIRA) that was recently developed in [2]. SAFIRA was built in a Lagrangian framework, which naturally incorporates two types of statistics on shape variations - deformation vectors and tensors - in the regularization term of the registration. This makes structural brain MRI registrations more accurate and biologically realistic. Here, we add to the understanding of the energetic behavior of the system through looking at its Hamiltonian. Furthermore, we compare the vector-statistics version to the non-statistical one and to the widely-used fluid registration, which is based on the Navier-Stokes equation. For the statistical registration, we use prior information on a training set independent from the dataset to be analyzed. Registration accuracy is measured on a pre-labeled data set for all 3 methods, and we also compute the heritability of brain structure using 46 twin pairs. SAFIRA detected genetic effects more extensively and showed improved registration accuracy compared to the other two algorithms.

1 Introduction

Nonlinear registration is the warping of one object onto another, using measures of image similarity or corresponding features extracted from the images to guide the deformation. It is widely used in brain imaging for computational anatomy studies. Tensor-based morphometry (TBM), for example, identifies systematic differences in brain structure by statistically analyzing deformations that align images from many subjects to a common template.

Registration methods commonly combine two terms: a similarity measure (distance or measure of agreement between two images) that drives the transformation and a regularizer that ensures its smoothness. This extra term is added to the registration function being optimized, to enforce desirable transformation properties such as smoothness, invertibility and inverse-consistency. For instance, the similarity criterion is regarded as a body force introduced into mechanical equations that govern linear elastic motion (Hooke's Law) in [1] or viscous fluid equations (Navier-Stokes equation) in [4]. Other algorithms rely on Gaussian filtering [17] or enforce particular properties of the deformation such as diffeomorphic trajectories [10].

When registering structural magnetic resonance brain images, the information available (voxel intensity, pre-defined landmarks) is rather limited and correspondence mappings are not unique. Consequently, a realistic model is needed to achieve deformations that are closer to an independently defined ground truth. This can be done for instance, as we chose to do here, by incorporating statistical information on the data set into the deformation. Some registration methods

have been developed to encode information on the natural variability in brain structure [7], but none of the 14 most widely used methods incorporates statistical information, except in the form of stationary Laplacian-type priors that only enforce smoothness [8]. However, in [5], the authors nonlinearly rescaled statistics on the strain tensors to use them in a demons-like registration algorithm.

In [2], we implemented a Statistically-Assisted Fluid Registration Algorithm (SAFIRA). The non-statistical version of SAFIRA is the fluid equivalent of the elastic registration first introduced in [11], where the standard Euclidean elastic regularizer was replaced by one based on Riemannian metrics. The algorithm was re-formulated using the Lagrangian formalism to describe the dynamics of the system. This new formulation made it clear how to include the different types of statistics on the expected deformations [3]. The version of SAFIRA using statistics on the displacements was shown to give more accurate registrations and better detection sensitivity in a group-wise statistical analysis [3]. For those tests, the prior information was extracted from the dataset that is being analyzed.

Here we build on this work in two ways. First, we look at the system in the energy domain by building the Hamiltonian of the system, to better understand the transfer of energy between the different components of the registration equation. Secondly, we present extensive tests of SAFIRA, by comparing the more advantageous statistical version of the algorithm against other fluid registration algorithms such as the standard Navier-Stokes fluid algorithm [4] [9], and the non-statistical version of SAFIRA. However, to verify the independent effect of the prior information on the deformation, we use statistics computed from another dataset comparable to the one studied. Indeed, our tests were done using two data sets: the manually-labeled $LPBA40$, which is one of the standard datasets used in the field to compare the accuracy and precision of different registration algorithms [8] and a $3D$ dataset consisted of 23 pairs of identical twins and 23 pairs of same-sex fraternal twins. As both groups are composed of healthy young adults, each of them can serve as a training set when using the statistical version of the algorithm to register the subjects from the other group to a given template. The vector-based statistical algorithm is shown to perform better in terms of accuracy and detection. We also investigate the detection power of each algorithm via heritability measures on the twins dataset.

2 Defining SAFIRA

2.1 Introduction

A $3D$ brain image volume may be regarded as embedded in a deformable continuum-mechanical system for which each voxel is seen as a particle [4, **?**]. The system is then solved using a Newtonian mechanics equation of the form:

$$\frac{d\dot{q}(x,t)}{dt} = \nabla_q Cost - \alpha \nabla_{\dot{q}} Reg(\dot{q}) - \beta \dot{q}, \tag{1}$$

where $Cost = Sim(I, J \circ q) = \int (I(x) - J(q(x))^2 dx$ is the similarity criterion, here the sum of squared intensity differences (SSD) and Reg is the regularizing term. $\dot{q}$ is obtained from equation (1) at each time step Δt and integrated over time

to find the displacement q. It is not immediately clear how to include statistical information into this equation, hence the need for the Lagrangian formalism.

2.2 The generalized Lagrangian

When a system is subjected to conservative and non-conservative forces, the path followed by a mechanical system minimizes the action $\mathcal{S}$, defined as

$$\delta\mathcal{S} = \int_{t_0}^{t_1} \delta q \left(\frac{\partial L}{\partial q} - \frac{d}{dt}\frac{\partial L}{\partial \dot{q}} + \boldsymbol{F}.\frac{\partial \boldsymbol{r}}{\partial q} \right) dt, \tag{2}$$

where $L(q, \dot{q}) = T(\dot{q}) - V(q)$ is the conservative Lagrangian accounting for the kinetic and the potential energies ($T(\dot{q})$ and $V(q)$, respectively) and $\boldsymbol{F}$ is the nonconservative force during the virtual displacement $\delta\boldsymbol{r}$, q is the displacement and $\dot{q}$, the velocity. ,

$$\left(\frac{\partial L}{\partial q} \right) - \frac{d}{dt}\left(\frac{\partial L}{\partial \dot{q}} \right) + \boldsymbol{F}.\left(\frac{\partial \boldsymbol{r}}{\partial q} \right) = 0 \tag{3}$$

A complete derivation can be found for example in [16]. This dynamic equation defines the motion of the non-conservative system at each time t.

2.3 Defining SAFIRA

In this section, we use the Lagrangian theory presented in (2.2) to reformulate equation (1). Given the definition of the kinetic energy and acknowledging the conservative properties of the similarity term, the different terms of equation (1) may be defined as follows:

$$\text{Kinetic energy: } T = \frac{1}{2}||\dot{q}_j||_2^2 \qquad \text{Potential Energy: } V = Cost(q) \tag{4}$$
$$\text{Nonconservative energy: } V_{\boldsymbol{F}} = \alpha Reg(\dot{q}) + \frac{1}{2}\beta||\dot{q}||_2^2$$

In this case, by deriving each term of Eq. 4, one can verify that Eqs. 1 and 3 correspond to each other with:

$$\frac{d}{dt}\left(\frac{\partial L}{\partial \dot{q}_j} \right) = \frac{d\dot{q}}{dt} \qquad \frac{\partial L}{\partial q} = \nabla_q Cost(I, J, q) \tag{5}$$
$$\boldsymbol{F}\left(\frac{\partial \boldsymbol{r}}{\partial q} \right) = \alpha \nabla_{\dot{q}} Reg(\dot{q}) + \beta\dot{q}$$

This definition is used to find $\dot{q}$ at each time step. In the next section, we describe how statistical information is added to the non-conservative terms. This allows the system to dissipate more energy when it is moving in an expected direction (that agrees with this prior statistical information) or to keep or even inject energy when it is moving in an unlikely direction. This makes it easier to surpass local minima and keep moving towards a more plausible minimum.

2.4 Incorporating statistics

The two non-conservative terms in Eq. 4 can be modified to incorporate the covariance of the displacements and deformation matrices. First, the regularizer in our algorithm, here labeled as $Reg_{Riem}(\dot{q})$, can be modified to include statistics on the deformation tensors (see [3]). However, here we will focus only on the second non-conservative term, $\frac{1}{2}\beta||\dot{q}||_2^2$. The Euclidean norm $||.||_2$ in this term can be replaced by a Mahalanobis distance:

$$\boldsymbol{F}\left(\frac{\partial \boldsymbol{r}}{\partial q}\right) = \alpha\nabla_{\dot{q}} Reg_{Riem}(\dot{q}) + \beta\dot{q}_j^T cov_{q_j}^{-1}\dot{q}_j \tag{6}$$

with $cov_{q_j} = \frac{1}{N}\sum_i (q_i - \bar{q}_j)^T(q_i - \bar{q}_j)$, the covariance of the displacements q at a voxel j summed over the images i.

2.5 Implementation

SAFIRA is a multi-resolution algorithm. In the implementation, we neglects second order terms (hence, the equation used in practice is $\nabla_q Cost - \alpha\nabla_{\dot{q}} Reg(\dot{q}) - \beta\hat{\dot{q}} = 0$). Here $\hat{\dot{q}}$ represents the solution to either statistical or non-statistical versions (see 2.4). For each resolution:

1. Define a grid on the template and set $\dot{q}(\boldsymbol{x}, t = 0) = \mathbf{0}$. Then at each time step δt:
2. Calculate $\nabla_q Cost$
3. Solve the PDE to find $\dot{q}$ at each point in the grid, using a gradient descent (RK4). Here, $q(q, \dot{t} = 0) = \gamma G \circ \boldsymbol{F}$ with $\gamma = 0.3$ and G a Gaussian.
4. Find the time step using the user defined maximal flow allowed.
5. Integrate $\dot{q}$ to find the displacement q, within this time step.
6. Compute the Jacobian of the displacements. If the Jacobian determinant falls below 0.5, then re-grid the template and return to Step 4.
7. Obtain the new displacement field once the Jacobian value is acceptable.

Here, we do not use a traditional gradient descent but an explicit iterative method (RK4). This was chosen so that the resolution is less sensitive to local minima than a first-order method.

3 Hamiltonian mechanics: conservation of energy?

Using a Lagrangian structure makes each term easier to interpret. However, computing the corresponding Hamiltonian H is crucial to understand and characterize the interaction between the different energy terms. While the energy of conservative systems is maintained with t, this is no longer the case when non-conservative forces are added. In the context of registration, summarizing the transfers between the different types of energies is of considerable interest, as it can allow tuning of the local speed of registration.

The Hamiltonian H represents the energy of the conservative system and may be derived from the conservative Lagrangian L as

$$H = p\dot{q} - L \qquad \text{with} \qquad p = \left(\frac{\partial L}{\partial q}\right)_{q\dot{q}} \tag{7}$$

where p is the momentum of the system and q is the displacement. For non-conservative systems, we have

$$\dot{p} = \frac{d}{dt}\left(\frac{\partial L}{\partial q}\right)_{q\dot{q}} = \left(\frac{\partial L}{\partial q}\right) + \boldsymbol{F}\left(\frac{\partial \boldsymbol{r}}{\partial q}\right)$$

$$\text{Consequently,} \qquad \frac{dH}{dt} = \frac{d}{dt}(p\dot{q} - L) = \dot{p}\dot{q} + p\ddot{q} - \frac{\partial L}{\partial q}\dot{q} - \frac{\partial L}{\partial \dot{q}}\ddot{q} - \frac{\partial L}{\partial t}$$

$$\text{As in our case,} \quad \frac{\partial L}{\partial t} = 0, \qquad \frac{dH}{dt} = \dot{p}\dot{q} - \frac{\partial L}{\partial q}\dot{q}, \quad \text{we obtain :}$$

$$\frac{dH}{dt} = \boldsymbol{F}\left(\frac{\partial \boldsymbol{r}}{\partial q}\right)\dot{q} \tag{8}$$

For our system, $H = \alpha\nabla_{\dot{q}} Reg(\dot{q}) + \beta\hat{\dot{q}} - \frac{1}{2}||\dot{q}||^2 + Cost(q)$, so the kinetic and cost energies lost are transferred to the regularizer and dissipation terms over time. Hence, changing the weights of the different terms in the regularizer and the dissipation can change the speed at which the registration converges at each voxel.

4 Data and Analysis

4.1 Data Acquisition and preprocessing

The first dataset is composed of 3D structural brain MRI scans of 23 monozygotic (MZ) and 23 dizygotic (DZ) same-sex twin pairs (age range: $22-25$ years), as well as one scan from an identically scanned healthy subject used as the common target for the fluid registration. We collected $3D$ $T1$-weighted *MP-RAGE* images (with parameters $TR = 2500ms$, $TE = 3.83ms$, $TI = 1500ms$, flip angle $= 15^o$, coronal orientation, FOV $230mm$) on a 4 Tesla Brucker Medspec whole body scanner (Wesley Hospital, Brisbane, Australia). Non-brain tissue was deleted from the MRI images using the Brain Surface Extraction Software (*BSE*) [13] and linearly aligned to the Colin27 template. All scans were then aligned to the ICBM53 template using 9-parameter registration - *FMRIB*'s Linear Image Registration Toolbox, *FLIRT*, prior to the nonlinear registrations described in this paper. Secondly, the $LPBA40$ dataset contains 40 images (20 males and 20 females - average age 29.2 ± 6.3 yrs. Details can be found at `http://www.loni.ucla.edu/~shattuck/resources/lpba40/` . The volumes from the two datasets were intensity and space-normalized and resized to a common resolution.

4.2 Algorithms and data analysis

All subjects' 3D scans were non-linearly registered to a common template using the three algorithms (non-statistical and vector-statistics version of SAFIRA and traditional fluid). In each case, vector fields, and their corresponding Jacobian matrices J were computed at each voxel, resulting in a scalar value for the Jacobian determinant, $det(J)$. The $det(J)$'s express the local differences in volume ($3D$) or area ($2D$) between each subject and the target image: $detJ(\boldsymbol{u}) > 1$ indicates a local excess in the image being studied, compared to the template, while $detJ(\boldsymbol{u}) < 1$ indicates a local deficit.
In the case when the statistical algorithm was used, the prior information was computed from a first round of registration on the other dataset, i.e., all the LPBA40 volumes were registered to a common template, voxelwise displacement vectors were obtained for each subject, from which a voxelwise covariance matrix resulted. This statistical information was then incorporated in the deformation process when using the statistical version of the algorithm to register the twin images to the same template (and vice versa).

4.3 Genetic influence on brain structures

The detection power of the different algorithms, for use in a morphometry study, was compared by computing genetic measures from the twin dataset. To measure the resemblance between twin pairs, we first computed the intraclass correlation coefficient (ICC) for both the MZ and DZ groups in the cerebrum according to the equation: $ICC = \frac{\sigma_b^2}{(\sigma_b^2+\sigma_w^2)}$. σ_b^2 is the pooled variance between pairs and σ_w^2 is the variance within pairs [12]. From there, we computed the heritability $h^2 = 2(r(MZ)-r(DZ))$, where $r(MZ)$ and $r(DZ)$ are the intraclass correlation values for the MZ and DZ groups, respectively. Heritability is an estimate of the proportion of the observed variation in a measurement that is attributable to genetic differences among individuals.

4.4 Accuracy of volume quantification

As SAFIRA was primarily developed to study volume and shape differences between subjects as in TBM analyses, we estimated the accuracy of the three algorithms by measuring the volume differences in the 53 structures defined in the $LPBA40$ database. The differences were computed between one (randomly chosen) subject from the 40 subjects that was used as template, and each of the other 39 images registered to it. Briefly, the deformation field obtained from the registration of one subject's sMRI to the template is applied to the corresponding subject's labeled image and the labels of it are compared to the template's labeled image (the ground truth) (see [8] for more details).

5 Results

The heritability is displayed as a set of $3D$ maps for the whole cerebrum in the figure (*left*). The anatomical pattern is consistent overall for the 3 methods:

subcortical structures are shown to be influenced by genetic differences across individuals. However, the vector-based algorithm performs better compared to the traditional fluid and non-statistical version of SAFIRA. This is particularly notable in the occipital lobes, which have been found to be highly genetically influenced, perhaps as they mature early in life according to a consistent genetic program (white arrow). This can also be noticed in the prefrontal areas, where a high heritability is found by the statistical code only. These regions were previously shown to be related to IQ [14], which was shown to be partly heritable, according to the American Psychological Association. The heritability maps obtained with the statistical version also show less blurriness. On the right of the figure, we show the volume quantification error for all ROIs. Incorporating vector-based statistics on the deformation field during the registration improves volumetric matching for most delineated structures, and makes volume quantification more accurate. This is the especially clear for subcortical gray matter structures, such as the caudate and putamen.

6 Conclusion

Here, we thoroughly studied the vector-statistics version of SAFIRA and showed its advantages in terms of accuracy and sensitivity to genetic influences on brain structure. The results confirmed the findings of [3], where the prior information was provided by the same studied dataset. In particular, we compared it to the traditional fluid method commonly used in tensor-based morphometry, an application for which SAFIRA was primarily designed. More extensive genetic effects were detected with the statistical algorithm together with less noisy findings, maybe related to an improvement of the accuracy of the registration. We also computed the Hamiltonian of the system, which was crucial to understand the exchange of energy, and thus how the incorporation of statistics influences the deformation pattern.

References

1. Bajcsy R, Kovačič S,*Multiresolution elastic matching*, Computer vision, graphics and image processing, 46, (1989) 1-21
2. Anonymous, see Supplemental material 1.
3. Anonymous, see Supplemental material 2.
4. Christensen GE et al., *Deformable templates using large deformation kinematics*, IEEE Trans. Image Process. 5, (1996) 1435–1447
5. Commowick O et al., *Incorporating Statistical Measures of Anatomical Variability in Atlas-to-Subject Registration for Conformal Brain Radiotherapy*, MICCAI (2005), 927–934
6. Hulshoff Pol, HE et al., *Genetic Contributions to Human Brain Morphology and Intelligence*, J Neurosci 26, (2006) 10235–10242
7. Gee, JC, *On matching brain volumes*, Pattern Recognit, (1999)
8. Klein, A et al., *Evaluation of 14 nonlinear deformation algorithms applied to human brain mri registration*, NeuroImage 46, (2009) 786–802
9. Leporé N et al., *Tensor based morphometry using fast fluid registration an application to deafness*, SPIE (2008)

10. Miller MI, *Computational anatomy: shape, growth, and atrophy comparison via diffeomorphism*, Neuroimage 23, (2004) 19–33
11. Pennec, X et al., *Riemannian elasticity: A statistical regularization framework for non-linear registration*, MICCAI (2005) 943–950
12. Scout PE, Fleiss JL, *Intraclass correlations: Uses in assessing rater reliability*, Psychol Bull 2, (1979) 420–428
13. Shattuck, DW et al., *BrainSuite: an automated cortical surface identification tool*, MedIA 8, (2002) 129–141
14. Shawn, P et al., *Intellectual ability and cortical development in Children and Adolescent*, Nature 440, (2006) 676–678
15. Sowell E et al., *Mapping cortical change across the human life span*, Nat Neurosci 6, (2003) 309–315
16. Tveter, FT *Hamilton's equations of motion for non-conservative systems*, Celestial Mechanics and Dynamical Astronomy, 60 (1994) 409–419
17. Vercauteren T et al., *Symmetric Log-Domain Diffeomorphic Registration: A Demons-based Approach*, MICCAI (2008) 754–761

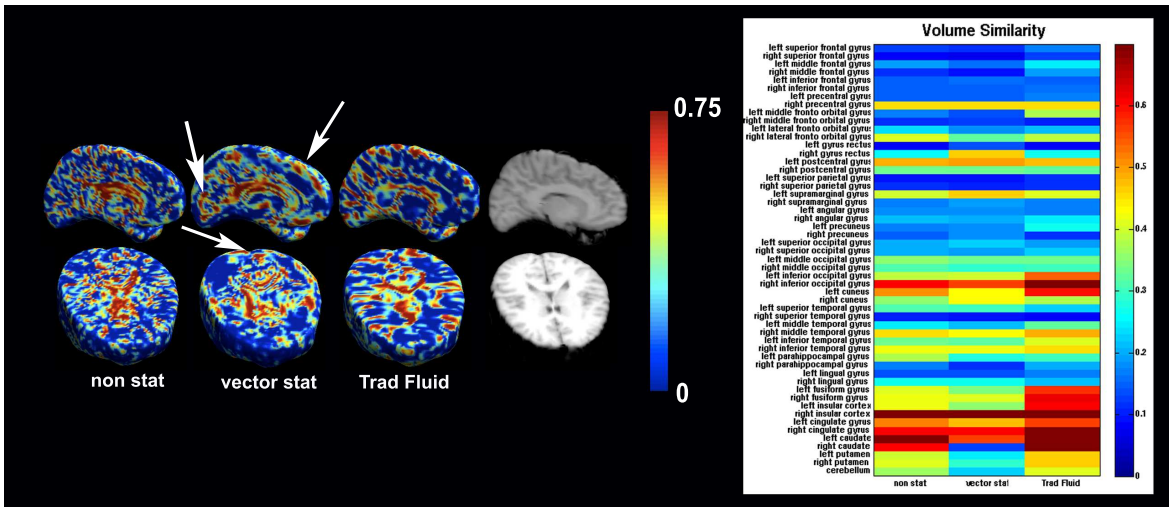

Fig. 1. Left: maps of heritability coefficients. Blue colors: $h^2 = 0$ no genetic influence - red colors: $h^2 = 0.75$ high heritability. **Right:** Volume Quantification Error. Blue shows a better registration accuracy.